scientific reports

Check for updates

OPEN

Vti1a/b support distinct aspects of TGN and *cis*-/medial Golgi organization

Danique M. van Bommel[1], Ruud F. Toonen[1] & Matthijs Verhage[1,2]✉

Retrograde trafficking towards the *trans*-Golgi network (TGN) is important for dense core vesicle (DCV) biogenesis. Here, we used Vti1a/b deficient neurons to study the impact of disturbed retrograde trafficking on Golgi organization and cargo sorting. In Vti1a/b deficient neurons, staining intensity of *cis*-/medial Golgi proteins (e.g., GM130 and giantin) was increased, while the intensity of two recycling TGN proteins, TGN38 and TMEM87A, was decreased and the TGN-resident protein Golgin97 was normal. Levels and localization of DCV cargo markers, LAMP1 and KDEL were also altered. This phenotype was not caused by reduced Golgi size or absence of a TGN compartment. The phenotype was partially phenocopied by disturbing sphingolipid homeostasis, but was not rescued by overexpression of sphingomyelin synthases or the sphingolipid synthesis inhibitor myriocin. We conclude that Vti1a/b are important for distinct aspects of TGN and *cis*-/medial Golgi organization. Our data underline the importance of retrograde trafficking for Golgi organization, DCV cargo sorting and the distribution of proteins of the regulated secretory pathway.

The Golgi complex is the major sorting organelle in the secretory pathway. It receives newly synthesized proteins from the endoplasmic reticulum and recycled cargo from other organelles, such as endosomes, by retrograde trafficking. In neurons, cargo leaving the Golgi apparatus can be sorted into constitutive or regulated secretory vesicles. Dense core vesicles (DCVs) are the main carriers of the regulated secretory pathway and contain neuropeptides and neurotrophins that modulate synaptic activity and play a role in the regulation of diverse functions such as fear, memory and appetite[1–3]. Alterations in neuropeptide/neurotrophin levels have been associated with pathological conditions such as anxiety, posttraumatic stress disorder and depression[4,5]. DCV cargo is synthesized at the endoplasmic reticulum and transported via the Golgi apparatus to the *trans*-Golgi network (TGN)[6]. How DCV cargo is sorted into DCVs and away from other secretory pathways at the TGN is poorly understood. Recent studies emphasize the importance of retrograde trafficking from endosomes to the TGN for DCV biogenesis[7,8], but the interplay between these pathways remains elusive.

Ma et al.[8] show that DCV maturation in larval salivary glands of *Drosophila melanogaster* requires retrograde transport from early endosomes. In addition, Vti1a/b, SNARE proteins involved in endosome-to-TGN retrograde trafficking, are necessary for DCV cargo sorting and exit from the Golgi[7]. Neurons that are deficient in Vti1a/b contain fewer DCVs and staining intensity of DCV cargo is reduced. Further experiments show that DCV cargo accumulates in the Golgi and that the heterogeneous distribution of DCV cargo in the Golgi is lost. The Golgi apparatus is more compact and Golgi morphology in electron micrographs is abnormal: its cisternae are distended and vacuoles are observed in the proximity of the Golgi. While transport of DCV cargo from the endoplasmic reticulum to the Golgi apparatus is normal, export of regulated cargo and, to a lesser extent, constitutive cargo from the TGN is reduced. It was proposed that the retrograde endosome-to-TGN pathway is crucial for retrieval of proteins involved in DCV biogenesis to the TGN. Characterizing the Golgi defects caused by loss of Vti1a/b in neurons will provide insight into the requirements for DCV biogenesis.

Here, we studied the impact of disturbed retrograde trafficking on the organization of the Golgi apparatus and proteins involved in Golgi export. For this goal, we used primary hippocampal neurons of Vti1a/b deficient mice and analyzed the localization and levels of *cis*-/medial Golgi and TGN proteins, and DCV cargo using confocal microscopy. We confirmed that the Golgi of Vti1a/b deficient neurons is condensed and that DCV cargo accumulates in the Golgi. Staining of Golgi-localized proteins was abnormal and levels and localization of proteins associated with DCVs were disturbed. Staining intensity of LAMP1-positive organelles was also

[1]Department of Functional Genomics, Center for Neurogenomics and Cognitive Research (CNCR), Vrije Universiteit (VU) Amsterdam, De Boelelaan 1085, Amsterdam 1081 HV, The Netherlands. [2]Functional Genomics, Department of Human Genetics, Center for Neurogenomics and Cognitive Research (CNCR), UMC Amsterdam, De Boelelaan 1085, Amsterdam 1081 HV, The Netherlands. ✉email: matthijs@cncr.vu.nl

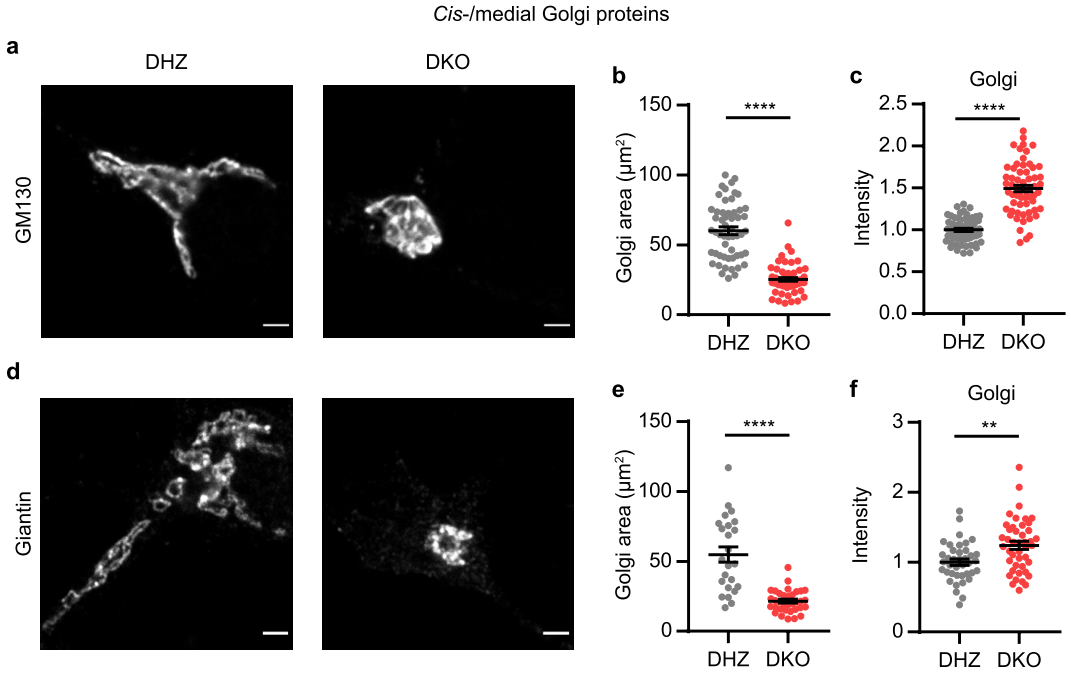

Figure 1. Staining intensity of *cis*-/medial Golgi proteins is increased in Vti1a/b deficient neurons. (**a**) Representative examples of neurons immunostained for GM130. (**b**) Decreased Golgi area based on GM130 staining in Vti1a/b DKO neurons (n = 66) compared to DHZ controls (n = 64). Mann Whitney test: ****p < 0.0001. (**c**) GM130 normalized staining intensity in the Golgi is increased (DHZ: n = 65, DKO: n = 61). *t*-test: ****p < 0.0001. (**d**) Representative examples of neurons immunostained for giantin. (**e**) Decreased Golgi area based on giantin staining in Vti1a/b DKO neurons (DHZ: n = 29; DKO: n = 39). *t*-test: ****p < 0.0001. (**f**) Giantin normalized staining intensity in the Golgi is increased (DHZ: n = 39; DKO: n = 44). *t*-test: **p = 0.0017. Bars show mean ± SEM. Detailed statistics are shown in Supplementary Table 1. Scale bar is 2 µm.

reduced and their shapes were altered. These defects were not caused by reduced Golgi area or the absence of a TGN compartment. The phenotype was partially mimicked by addition of ceramide or sphingosine to neurons, but not rescued by overexpression of sphingomyelin synthases or treatment with myriocin. We conclude that Vti1a/b are required for a normal *cis*-/medial Golgi and TGN and for a normal distribution of proteins involved in regulated secretion.

Results

To study the impact of disturbed retrograde trafficking on Golgi organization and proteins involved in Golgi export, we used mouse hippocampal neurons from Vti1a/b double knock-out (DKO), with double heterozygous (DHZ) mice as a control[7]. First, to confirm and extend the previously observed Golgi abnormalities, we examined levels and localization of two *cis*-/medial Golgi markers, five *trans*-Golgi network (TGN) proteins, two DCV cargoes and two proteins implicated in DCV biogenesis.

***Cis*-/medial Golgi and TGN protein staining is altered in Vti1a/b DKO neurons.** Previously, it was shown that the *cis*-Golgi marker GM130 stains a smaller area and its staining intensity is increased in the absence of Vti1a/b[7]. We confirmed these observations here (Fig. 1a–c). In addition, the area stained by giantin, a *cis*-/medial Golgi marker, was also smaller and its average staining intensity was higher in DKO neurons than in controls (Fig. 1d–f). To estimate the total amount of GM130 and giantin localized to the Golgi, we measured the integrated density of the markers by multiplying the mean gray value and the area of the region of interest. Even though the average staining intensities of GM130 and giantin were higher, the Golgi integrated densities of these proteins were lower (Supplementary Fig. 1a, b). These data confirm previous data and suggest that the expression levels of *cis*-/medial Golgi marker proteins are lower in the Golgi of Vti1a/b DKO neurons.

To examine the TGN, we used antibodies against the recycling TGN marker TGN38, the Golgi-resident marker Golgin97 and three other proteins that localize to the TGN: TMEM87A, ARL1 and gamma-adaptin (Fig. 2a, e, i, m, q). In contrast to *cis*-/medial Golgi markers, the average staining intensity of TGN proteins was decreased in the Golgi (Fig. 2b, f, j, r) or normal (Fig. 2n). The decrease was largest for TMEM87A, for which the average staining intensity in the Golgi was reduced by ~ 50%, compared to control neurons. Similar to *cis*-/medial Golgi proteins, Golgi integrated density of all five TGN proteins was decreased in Vti1a/b DKO neurons (Supplementary Fig. 1c–g). These data suggest that loss of Vti1a/b not only affects the level of *cis*-/medial Golgi proteins, but also of TGN proteins.

TGN38 shuttles between the plasma membrane and the TGN[9,10]. Since Vti1a/b are required for retrograde trafficking to the Golgi, TGN proteins might need Vti1a/b to return to the Golgi. Loss of Vti1a/b could thus have

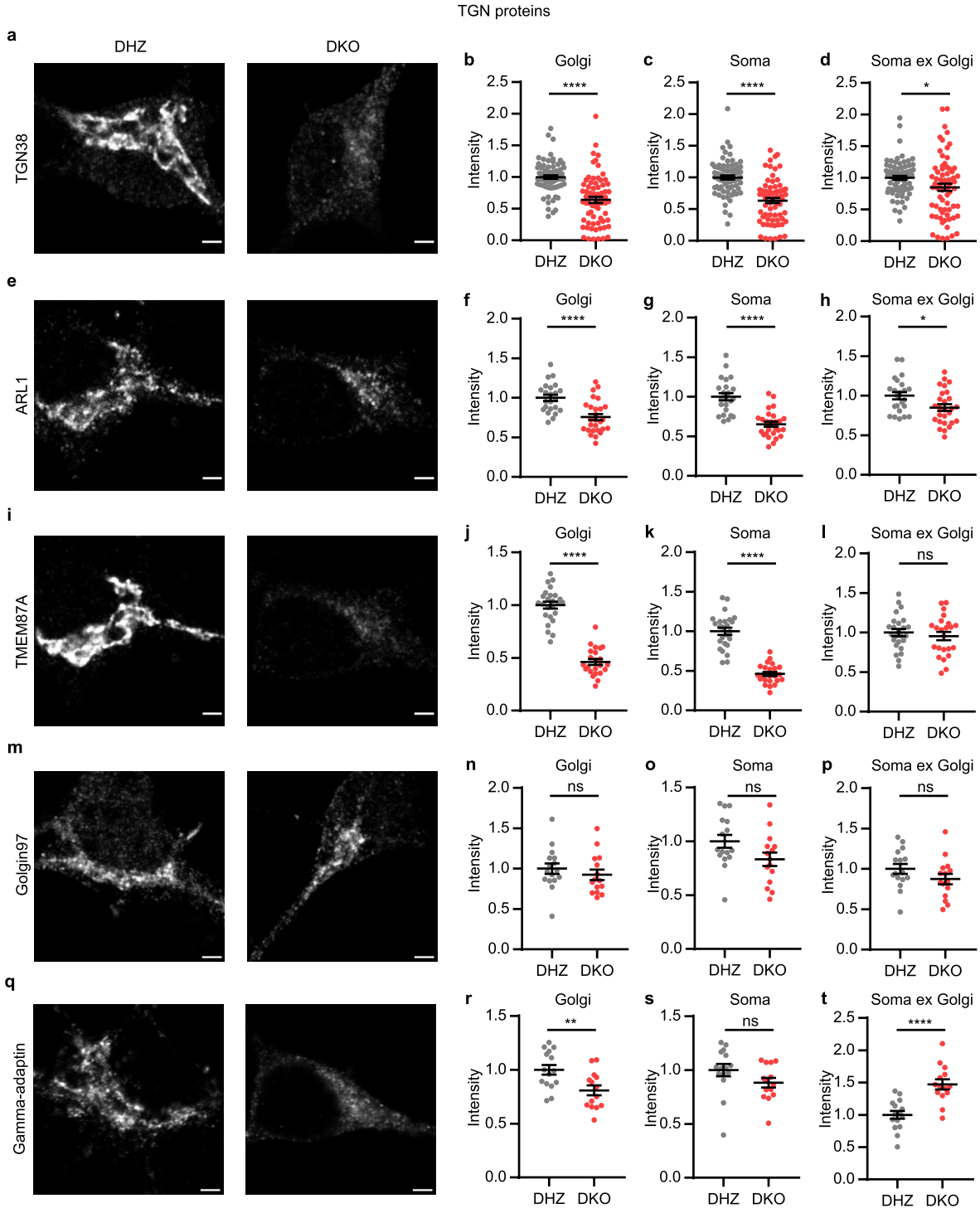

Figure 2. Staining intensity of TGN proteins is decreased or not affected in Vti1a/b deficient neurons. (**a**) Representative examples of neurons immunostained for TGN38. (**b**–**d**) TGN38 normalized staining intensity is decreased in the Golgi (Mann Whitney test: ****p < 0.0001) (**b**), soma (Mann Whitney test: ****p < 0.0001) (**c**), and soma excluding Golgi (Mann Whitney test: *p = 0.0145) (**d**) (DHZ: n = 73; DKO: n = 69). (**e**) Representative examples of neurons immunostained for ARL1. (**f**–**h**) ARL1 normalized staining intensity is decreased in the Golgi (*t*-test: ****p < 0.0001) (**f**), soma (*t*-test: ****p < 0.0001) (**g**), and soma excluding Golgi (*t*-test: *p = 0.0212) (**h**) (DHZ: n = 23; DKO: n = 27). (**i**) Representative examples of neurons immunostained for TMEM87A. (**j**–**l**) TMEM87A normalized staining intensity is decreased in the Golgi (*t*-test: ****p < 0.0001) (**j**) and soma (*t*-test: ****p < 0.0001) (**k**), but not significantly different in the soma excluding Golgi (*t*-test: ns, p = 0.5162) (**l**) (DHZ: n = 25; DKO: n = 23). (**m**) Representative examples of neurons immunostained for Golgin97. (**n**–**p**) Golgin97 normalized staining intensity is not affected in the Golgi (*t*-test: ns, p = 0.4196) (**n**), soma (*t*-test: ns, p = 0.0648) (**o**) or soma excluding Golgi (*t*-test: ns, p = 0.1673) (**p**) (DHZ: n = 16; DKO: n = 15). (**q**) Representative examples of neurons immunostained for gamma-adaptin. (**r**–**t**) Gamma-adaptin normalized staining intensity is decreased in the Golgi (*t*-test: **p = 0.0067) (**r**), not significantly different in the soma (Mann Whitney test: ns, p = 0.0568) (**s**), and increased in the soma excluding Golgi (t-test: ****p < 0.0001) (**t**) (DHZ: n = 15; DKO: n = 14). Bars show mean ± SEM. Detailed statistics are shown in Supplementary Table 1. Scale bar is 2 µm.

resulted in altered localization of TGN proteins. The average staining intensity of TGN38, ARL1 and TMEM87A was lower in the whole soma of DKO neurons when compared to control neurons, and it was normal for Golgin97 and gamma-adaptin (Fig. 2c, g, k, o, s). In addition, the staining intensity in the soma excluding the Golgi was not different for TMEM87A and Golgin97 and slightly decreased for TGN38 and ARL1 (Fig. 2d, h, l, p). In contrast, gamma-adaptin staining intensity in the soma excluding the Golgi was increased (Fig. 2t). Thus, gamma-adaptin might relocalize to the cytoplasm, but the decreased staining intensity of TGN38, ARL1 and TMEM87A in the Golgi of Vti1a/b DKO neurons is not caused by mislocalization to a different compartment in the soma. We tested antibodies for several TGN proteins to quantify total protein levels using Western blotting. Only Golgin97 and gamma-adaptin antibodies showed specific signals, with several unidentified smaller bands for gamma-adaptin (Supplementary Fig. 2, Supplementary Fig. 3). These results were in line with our observations based on immunofluorescence.

Reduced staining intensity of TGN38, TMEM87A and ARL1 could also be the result of epitope masking. To examine this possibility, TGN38-GFP was overexpressed in Vti1a/b DKO and control neurons and GFP fluorescence intensity in the Golgi was measured. The decrease in intensity of TGN38-GFP was similar to endogenous TGN38 (Supplementary Fig. 4, Fig. 2b). This rules out epitope masking as an explanation of reduced TGN38 staining intensity. Taken together, total levels of all analyzed Golgi proteins are decreased in the Golgi of Vti1a/b DKO neurons. While staining intensity of *cis*-/medial Golgi proteins is increased, the staining intensity of TGN proteins is decreased or not affected.

Levels and localization of DCV markers are altered in Vti1a/b DKO neurons. We continued by analyzing proteins associated with DCVs. CgB and NPY-SEP are established endogenous and heterologous DCV markers, respectively[11,12]. As shown before, NPY-SEP intensity in the Golgi was not significantly different in the absence of Vti1a/b (DHZ vs DKO, $p = 0.0567$; Fig. 3m, n)[7]. In contrast, CgB staining intensity in the Golgi was increased (Fig. 3a, b).

The increased CgB staining intensity suggests that endogenous DCV cargo accumulated in the Golgi. However, the total Golgi area was smaller in Vti1a/b DKO neurons (Fig. 1). Indeed, the integrated density (mean gray value multiplied by the total Golgi area) of both proteins was reduced (Supplementary Fig. 1h, i). Hence, although CgB staining intensity was higher, the total amount of CgB staining (and NPY fluorescence) in the Golgi was in fact lower, arguing against cargo accumulation in the Golgi. In the soma (in general, and specifically the soma excluding the Golgi) NPY-SEP intensity was lower in Vti1a/b DKO neurons (Fig. 3o, p), while CgB staining intensity was higher (Fig. 3c, d). This shows that Golgi levels of DCV cargo are decreased in the absence of Vti1a/b, but that the effects on localization are different for CgB and NPY-SEP.

HID1 and CCDC186 play a role in the biogenesis/maturation of DCVs[13,14]. Similar to most TGN proteins, HID1 Golgi staining intensity was decreased in the Golgi, and in the whole soma (Fig. 3e–h). CCDC186 staining intensity was not different in the Golgi, while it was decreased in the whole soma (Fig. 3i–l). The integrated density of both proteins in the Golgi was reduced (Supplementary Fig. 1j, k). For CCDC186, Western blot results were in line with these observations (Supplementary Fig. 2, Supplementary Fig. 3). Taken together, the levels and localization of proteins associated with DCVs are all altered by the absence of Vti1a/b, but the effects are different for different proteins.

LAMP1 carrier and KDEL staining are altered in Vti1a/b deficient neurons. Since the whole Golgi is disturbed by loss of Vti1a/b, we hypothesized that abnormal staining patterns are not restricted to DCVs and also exist for other types of vesicles, such as LAMP1 carriers. Indeed, compared to control neurons, Vti1a/b DKO neurons showed lower levels of LAMP1 staining intensity and the shape of these carriers was different (Fig. 4a, b). Control neurons contained characteristic oval shapes, while DKO neurons contained significantly fewer ovals (Large ovals DHZ vs DKO, $p < 0.0001$, Total ovals DHZ vs DKO, $p < 0.0001$; Fig. 4c, d). These results indicate that Vti1a/b are required for normal LAMP1 localization and levels. In addition, staining intensity of the ER marker KDEL was decreased (Supplementary Fig. 5). Taken together, loss of Vti1a/b does not only affect the Golgi apparatus and DCVs, but also LAMP1 carriers and the ER.

Golgi abnormalities in Vti1a/b DKO neurons are not caused by reduced Golgi area or absence of a TGN compartment. Next, we investigated how loss of Vti1a/b causes disorganization of the ER, Golgi apparatus, DCVs and LAMP1 carriers. We hypothesized that the absence of Vti1a/b leads to a smaller Golgi, which is not large enough to achieve normal Golgi function. In wildtype neurons, the Golgi grows significantly between DIV2 and DIV3[15]. Therefore, if Golgi size is the main cause of the Vti1a/b DKO phenotype, control neurons at DIV2 should show a similar phenotype to Vti1a/b DKO neurons. As expected, at DIV2, the Golgi area of control neurons was smaller than at DIV8 (Supplementary Fig. 6a, b, Fig. 1b, e). The difference between control and DKO Golgi area at DIV2 was much smaller than the difference at DIV8. However, Golgi staining intensities of DKO neurons were affected similar to DIV8 neurons, when compared to controls (Supplementary Fig. 6, Figs. 1, 2). This excludes Golgi size as a plausible cause for the Vti1a/b DKO phenotype.

Subsequently, we tested whether TGN38 reaches the TGN in Vti1a/b DKO neurons. To test this, we overexpressed TGN38-GFP and stained for *cis*-Golgi marker GM130 and TGN protein TMEM87A. Line scans showed that the peak of intensity of TGN38-GFP was well separated from the peak of GM130 and close to the peak of TMEM87A (Fig. 5). No significant difference between control and Vti1a/b DKO neurons was observed (DHZ GM130 vs DKO GM130, $p = 0.3769$, DHZ TMEM87A vs DKO TMEM87A, $p = 0.9976$). This suggests that TGN38-GFP can reach a TGN compartment in absence of Vti1a/b. Taken together, Golgi abnormalities in Vti1a/b DKO neurons are not caused by reduced Golgi size or the absence of a TGN compartment.

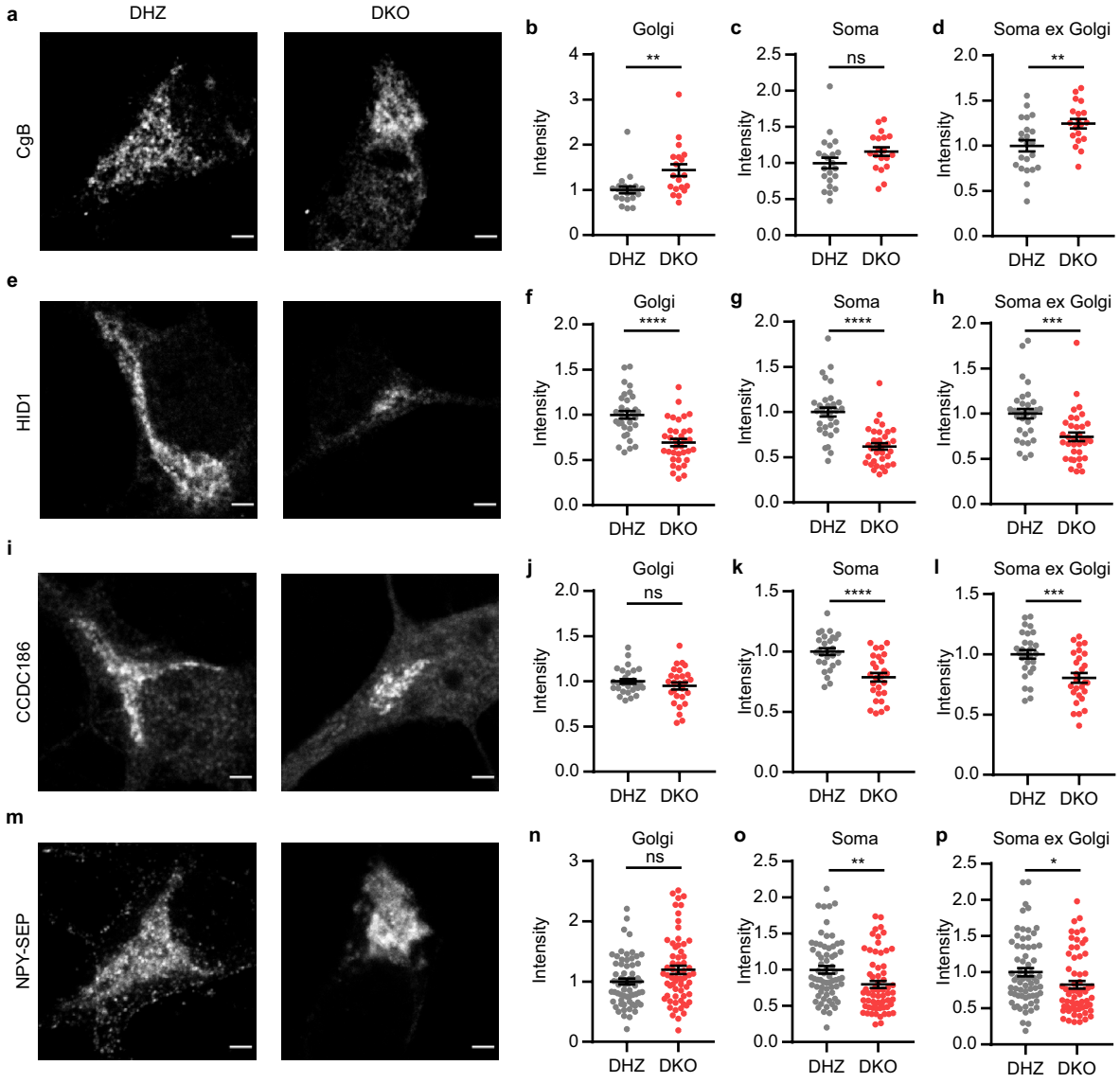

Figure 3. Levels and localization of DCV proteins are affected in Vti1a/b DKO neurons. (**a**) Representative examples of neurons immunostained for CgB. (**b**–**d**) CgB normalized staining intensity is increased in the Golgi (Mann Whitney test: **p = 0.0024) (**b**), not significantly different in the soma (*t*-test: ns, p = 0.1142) (**c**), and increased in the soma excluding Golgi (*t*-test: **p = 0.0056) (**d**) (DHZ: n = 22; DKO: n = 19). (**e**) Representative examples of neurons immunostained for HID1. (**f**–**h**) HID1 normalized staining intensity is decreased in the Golgi (*t*-test: ****p < 0.0001) (**f**), soma (Mann Whitney test: ****p < 0.0001) (**g**), and soma excluding Golgi (Mann Whitney test: ***p = 0.0001) (**h**) (DHZ: n = 32; DKO: n = 35). (**i**) Representative examples of neurons immunostained for CCDC186. (**j**–**l**) CCDC186 normalized staining intensity is not significantly different in the Golgi (*t*-test: ns, p = 0.2927) (**j**), but decreased in the soma (*t*-test: ****p < 0.0001) (**k**), and soma excluding Golgi (*t*-test: ***p = 0.0006) (**l**) (DHZ: n = 28; DKO: n = 27). (**m**) Representative examples of neurons expressing NPY-SEP. (**n**–**p**) NPY-SEP normalized fluorescence intensity is not significantly different in the Golgi (Mann Whitney test: ns, p = 0.0567) (**n**), but decreased in the soma (Mann Whitney test: **p = 0.0016) (**o**), and soma excluding Golgi (Mann Whitney test: *p = 0.0111) (**p**) (DHZ: n = 67; DKO: n = 64). Bars show mean ± SEM. Detailed statistics are shown in Supplementary Table 1. Scale bar is 2 µm.

Vti1a/b DKO Golgi abnormalities are partially phenocopied by disturbing membrane homeostasis. Having ruled out reduced Golgi size as an explanation for the Vti1a/b DKO phenotype, we hypothesized that membrane homeostasis is disturbed in Vti1a/b DKO neurons. Previous research showed that addition of C6-Ceramide to HeLa cells and NRK cells results in distended Golgi cisternae, similar to what was observed in Vti1a/b DKO neurons[7,16,17]. Further experiments showed that sphingosine, a metabolite of ceramide, causes these effects[16]. We mimicked disturbed membrane homeostasis by addition of C6-Ceramide or L-Erythro-Sphingosine to wildtype neurons. C6-Ceramide can be metabolized, while L-Erythro-Sphingosine is a nonmetabolizable stereoisomer. After 4 h incubation with C6-Ceramide or L-Erythro-Sphingosine, the Golgi

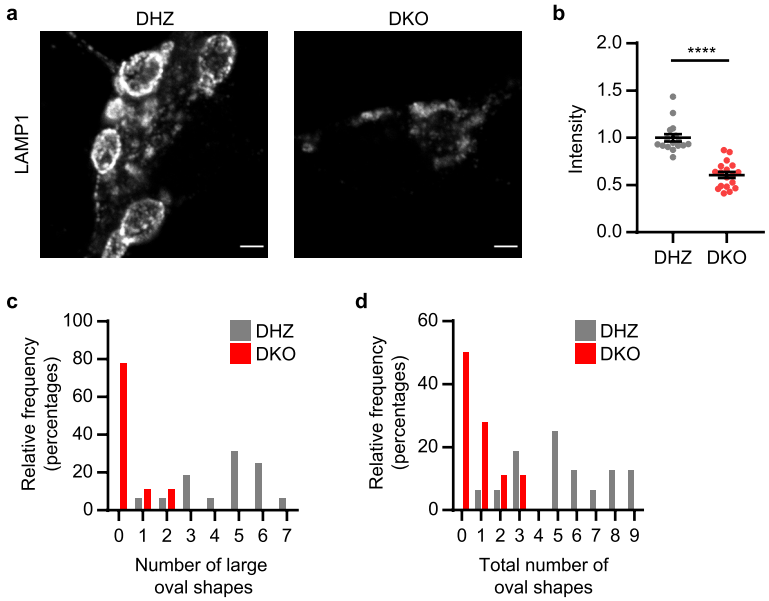

Figure 4. LAMP1 staining intensity and shape are abnormal in Vti1a/b deficient neurons. (**a**) Representative examples of neurons immunostained for LAMP1. (**b**) Normalized staining intensity of LAMP1 is decreased in Vti1a/b DKO neurons compared to DHZ neurons (DHZ: n = 16; DKO: n = 18). Mann Whitney test: ****p < 0.0001. (**c**) Number of large, clear oval LAMP1 shapes is decreased in Vti1a/b deficient neurons (DHZ: n = 16; DKO: n = 18). Mann Whitney test: ****p < 0.0001. (**d**) Total number of oval LAMP1 shapes (including less distinguished ovals) is decreased in Vti1a/b deficient neurons (DHZ: n = 16; DKO: n = 18). Mann Whitney test: ****p < 0.0001. Bars show mean ± SEM. Detailed statistics are shown in Supplementary Table 1. Scale bar is 2 µm.

was fragmented (Fig. 6a, b). Staining intensity for *cis*-Golgi marker GM130 was normal, but was decreased for both TGN proteins TGN38 and TMEM87A (Fig. 6). Since Golgi fragmentation was not observed in Vti1a/b DKO neurons, we conclude that disturbed membrane homeostasis cannot fully explain the Vti1a/b DKO phenotype, despite the fact that GM130, TMEM87A and TGN38 were similarly affected in Vti1a/b DKO neurons as in neurons treated with L-Erythro-Sphingosine or C6-Ceramide.

Vti1a/b DKO Golgi abnormalities are not rescued by overexpression of sphingomyelin synthases or addition of myriocin. Similar to Vti1a/b DKO, deficiency of any of the components of the Conserved Oligomeric Golgi (COG) complex impacts retrograde trafficking, and morphology and function of the Golgi[18,19]. Experiments in COG KD cells showed mislocalization of sphingomyelin synthase 1 (SMS1), the enzyme that converts ceramide into sphingomyelin[20]. It is conceivable that Vti1a/b are required for recycling of SMS1 to the Golgi. Two commercially available antibodies failed to produce reliable immunocytochemical stainings, precluding the analysis of endogenous SMS1 distribution in the absence of Vti1a/b. In addition to SMS1, which is mainly localized to the Golgi, sphingomyelin synthase 2 (SMS2) is found on the plasma membrane and in the Golgi[21,22]. To visualize SMS1 and SMS2 in Vti1a/b DKO neurons, we tagged both with GFP. Similar to other TGN proteins, the intensity of SMS1-GFP and SMS2-GFP was lower in the Golgi of Vti1a/b DKO neurons as compared to Vti1a/b neurons, but no additional abnormalities were identified (Supplementary Fig. 7). If the Golgi phenotype in Vti1a/b deficient neurons was the result of mislocalization of SMS1 or SMS2, overexpression of these proteins could rescue the phenotype. However, while SMS1-GFP and SMS2-GFP were correctly targeted to the TGN, the Golgi area remained small and TMEM87A intensity remained low (Supplementary Fig. 7). Thus, overexpression of SMS1-GFP or SMS2-GFP does not rescue the Vti1a/b DKO phenotype.

Deficiency of subunits of the GARP (Golgi-associated retrograde protein) complex also leads to retrograde trafficking defects and distended Golgi cisternae[23,24], resembling Golgi abnormalities in Vti1a/b DKO neurons. Myriocin is an inhibitor of sphingolipid synthesis and was shown to rescue GARP deficiency in vitro and in vivo[25,26]. We tested whether myriocin rescued Golgi abnormalities in Vti1a/b DKO neurons. Application of myriocin led to a trend towards an increased Golgi area at DIV7 ($p = 0.159$), and did not rescue the decreased TMEM87A staining intensity in Vti1a/b DKO neurons (Figs. 1, 7). Hence myriocin does not rescue the Vti1a/b DKO phenotype.

Discussion

We investigated the role of retrograde trafficking in the organization of the Golgi apparatus and proteins involved in Golgi export. We showed that *cis*-/medial Golgi and TGN are affected differentially by the loss of Vti1a/b. This phenotype could not be explained by reduced Golgi size or absence of (one of) the TGN compartment(s), but

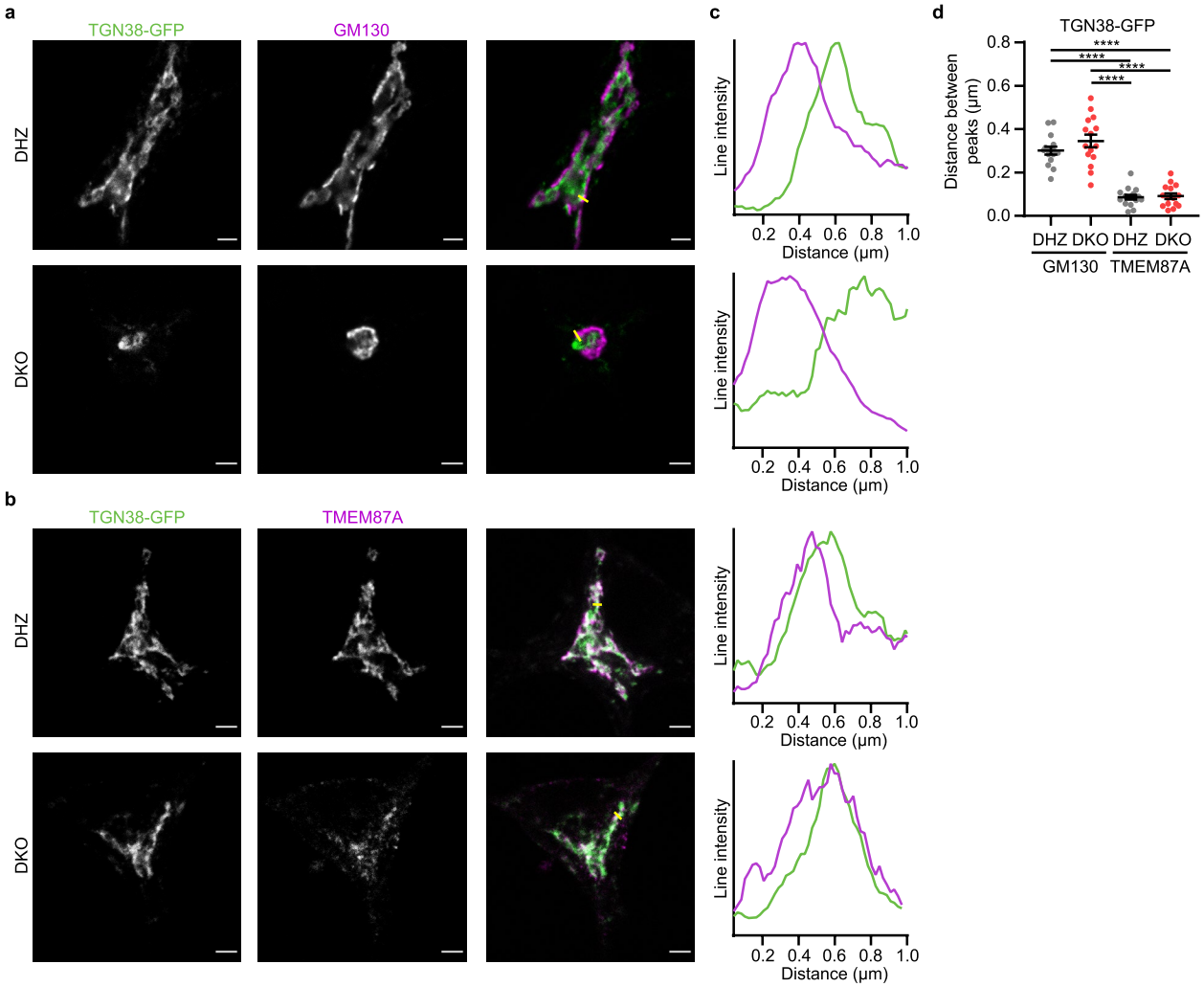

Figure 5. TGN38-GFP can reach the TGN compartment in Vti1a/b DKO neurons. (**a**) Representative examples of neurons overexpressing TGN38-GFP immunostained for GM130. (Brightness and contrast have been adjusted for visualization). (**b**) Representative examples of neurons overexpressing TGN38-GFP immunostained for TMEM87A. (Brightness and contrast have been adjusted for visualization). (**c**) Intensity profiles of TGN38-GFP and GM130/TMEM87A. Location of lines is represented as a yellow line in merged images. Intensities were normalized and smoothed before plotting. (**d**) The distance between intensity peaks of TGN38-GFP and GM130 is larger than the distance between peaks of TGN38-GFP and TMEM87A in both Vti1a/b DHZ and DKO neurons, measured by line scans through the Golgi (DHZ GM130: n = 15; DKO GM130: n = 15; DHZ TMEM87A: n = 15; DKO TMEM87A: n = 15). One way ANOVA with Tukey's multiple comparisons test: DHZ GM130 vs DHZ TMEM87A, DHZ GM130 vs DKO TMEM87A, DKO GM130 vs DHZ TMEM87A and DKO GM130 vs DKO TMEM87A: ****$p < 0.0001$, DHZ GM130 vs DKO GM130 and DHZ TMEM87A vs DKO TMEM87A: non-significant (ns). Bars show mean ± SEM. Detailed statistics are shown in Supplementary Table 1. Scale bar is 2 μm.

was partially mimicked by addition of C6-Ceramide or L-Erythro-Sphingosine. The phenotype was not rescued by overexpression of sphingomyelin synthases or myriocin treatment.

Loss of Vti1a/b results in reduced Golgi area in neurons[7]. For *cis*-/medial Golgi proteins, the integrated density (total area multiplied by the average staining intensity) was decreased, while at the same time the average intensity was increased. This suggests that the total protein level is lower, but the proteins that are present, are in a smaller area, causing a relative increase in intensity. TGN proteins showed lower integrated density and lower or similar average intensity in the Golgi. This indicates that total protein expression levels are decreased and this cannot be fully explained by a smaller Golgi area. Western blotting results for gamma-adaptin and Golgin97 were in line with these observations. Golgin97 was the only TGN protein for which the average Golgi intensity was not affected in Vti1a/b DKO neurons, while Golgi intensity was reduced for TGN38, TMEM87A, ARL1 and gamma-adaptin. This suggests that Golgin97 is differentially affected by loss of Vti1a/b than the other four TGN proteins. Golgin97 is one of the Golgins that is recruited to the Golgi by ARL1[27]. Since ARL1 Golgi intensity was decreased (but not absent) the residual ARL1 might be enough to recruit Golgin97 to the Golgi. Taken together, TGN proteins are more severely affected by loss of Vti1a/b than *cis*-/medial Golgi proteins.

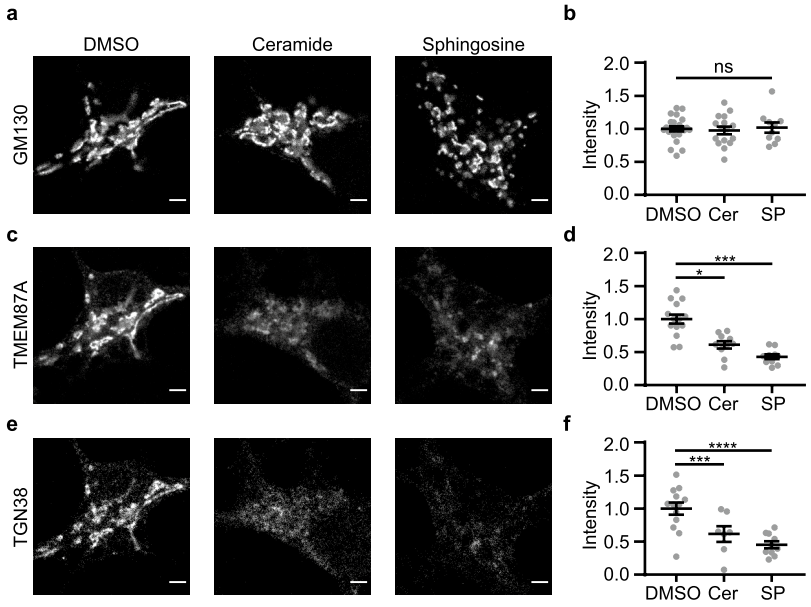

Figure 6. Addition of C6-Ceramide (Cer) or L-Erythro-Sphingosine (SP) to wildtype neurons does not affect staining intensity of *cis*-Golgi protein GM130, while TGN protein staining intensity is decreased. (**a**) Representative examples of neurons immunostained for GM130, after 4 h treatment with 0.1% DMSO, 20 µM C6-Ceramide or 8 µM L-Erythro-Sphingosine. (**b**) GM130 normalized staining intensity is not affected by C6-Ceramide or L-Erythro-Sphingosine treatment (DMSO: n = 22; Cer: n = 16; SP: n = 10). One-way ANOVA (ns, p = 0.8834). (**c**) Representative examples of neurons immunostained for TMEM87A, after 4 h treatment with 0.1% DMSO, 20 µM C6-Ceramide or 8 µM L-Erythro-Sphingosine. (**d**) TMEM87A normalized staining intensity is decreased after C6-Ceramide or L-Erythro-Sphingosine treatment (DMSO: n = 14; Cer: n = 10; SP: n = 10). One-way ANOVA with Tukey's multiple comparisons test: DMSO vs Cer: ***p = 0.0002, DMSO vs SP: ****p < 0.0001, Cer vs SP: ns, p = 0.1312. (**e**) Representative examples of neurons immunostained for TGN38, after 4 h treatment with 0.1% DMSO, 20 µM C6-Ceramide or 8 µM L-Erythro-Sphingosine. (**f**) TGN38 normalized staining intensity is decreased after C6-Ceramide or L-Erythro-Sphingosine treatment (DMSO: n = 13; Cer: n = 7; SP: n = 10). One-way ANOVA with Tukey's multiple comparisons test: DMSO vs Cer: *p = 0.0186, DMSO vs SP: ***p = 0.0002, Cer vs SP: ns, p = 0.4809. Bars show mean ± SEM. Detailed statistics are shown in Supplementary Table 1. Scale bar is 3 µm.

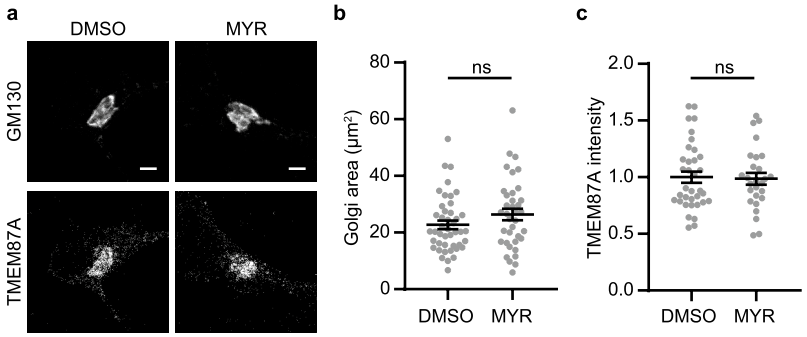

Figure 7. Addition of myriocin (MYR) to Vti1a/b DKO neurons does not rescue Golgi area or TGN staining intensity. (**a**) Representative examples of neurons immunostained for GM130 and TMEM87A, after 1 week treatment with 0.1% DMSO or 50 µM Myriocin. (**b**) Golgi area based on GM130 is not affected by myriocin treatment (DMSO: n = 44; MYR: n = 37). Mann Whitney test: ns, p = 0.1593. (**c**) TMEM87A normalized staining intensity is not affected by myriocin treatment (DMSO: n = 35; MYR: n = 27). Mann Whitney test: ns, p = 0.8546. Bars show mean ± SEM. Detailed statistics are shown in Supplementary Table 1. Scale bar is 3 µm.

The differential effect between *cis*-/medial Golgi and TGN proteins may be explained assuming that defective retrograde trafficking to the TGN affects TGN proteins more directly than *cis*-/medial Golgi proteins. If TGN proteins do not return to the TGN, they are expected to accumulate outside the Golgi. By measuring the staining intensity in the rest of the soma, we ruled out that TGN38, TMEM87A and ARL1 were accumulating there. Only gamma-adaptin was redistributed to the cytoplasm. It is possible that TGN38, TMEM87A and ARL1

are degraded when they cannot return to the Golgi, resulting in decreased protein levels. Western blot analysis detected smaller fragments of gamma-adaptin in Vti1a/b DKO neurons, suggesting it is being degraded. Thus, it is possible that proteins that cannot be recruited or returned to the Golgi are partially degraded, resulting in lower protein levels in the Golgi. Alternatively, epitope masking might explain decreased levels of four TGN proteins. For example, a defect in protein maturation could result in the antibody not binding its epitope. Since overexpressed TGN38-GFP intensity was decreased to the same extent as endogenous TGN38, we excluded epitope masking as an explanation, at least for TGN38. In addition, the TGN38 antibody used in this study also detected overexpressed TGN38-GFP in Vti1a/b DKO neurons, indicating that the epitope is available in mutant neurons. Several gene inactivation experiments or treatments are known to disturb Golgi morphology, similar but not identical to the observed effects in Vti1A/B DKO neurons. For example, brefeldin A (BFA) causes redistribution of Golgi proteins to the ER and induces tubulation of the TGN[28]. However, BFA leads to reduced staining intensity of *cis*-/medial Golgi proteins, while it was increased in Vti1a/b DKO and no TGN tubulation was observed. Rab30 deficiency also causes dispersal of TGN proteins, but causes only a mild perturbation of *cis*-Golgi protein GM130[29]. Furthermore, ARL1 is important for maintenance of Golgi morphology[30]. It recruits Golgins to the Golgi and is required for a normal TGN structure[27]. Overexpression of dominant negative ARL1 leads to reduced levels of *cis*-Golgi protein GS28, but has no effect on GM130[30–32]. Since intensity of *cis*-/medial Golgi proteins is increased in Vti1a/b DKO neurons, loss of ARL1 cannot fully explain the Vti1a/b DKO phenotype. Finally, Chia et al. performed an RNAi screen in HeLa cells for perturbations of Golgi morphology[33]. They identified many genes of which depletion resulted in diffuse signals for *trans*-Golgi proteins, but in those cases *cis*-Golgi proteins were also affected to a similar extent. We are not aware of studies describing other gene depletions or treatments that result in reduced or normal TGN staining but increased, condensed *cis*-/medial Golgi staining.

All proteins associated with DCVs showed decreased integrated density in the Golgi in absence of Vti1a/b, indicating that the levels of these proteins were reduced. As previously reported, the average intensity of NPY-SEP in the Golgi was not affected by loss of Vti1a/b, although a trend towards an increase was observed[7]. Golgi intensity of the endogenous DCV protein CgB was increased in the Golgi. Since protein levels were lower, this increase in average intensity was not caused by accumulation of CgB in the Golgi, but by reduction of Golgi size. While the intensity outside the Golgi apparatus was decreased for NPY-SEP, the intensity of CgB outside the Golgi increased. This could be explained by CgB being an endogenous and NPY-SEP a heterologous DCV marker, or it could be a difference between two DCV cargoes. It has been shown that CgB not only localizes to DCVs, but also to the nucleus in several cell types, including neuroendocrine cells, and plays a role in transcription[34]. Golgi stress in Vti1a/b DKO neurons could target CgB to the nucleus to induce changes in transcription. HID1 is thought to regulate DCV biogenesis in the TGN or DCV maturation by facilitating homotypic fusion[13,35]. Like other TGN proteins, HID1 intensity inside and outside the Golgi was lower in Vti1a/b DKO neurons. This suggests that HID1 is indeed localized to the TGN. CCDC186 Golgi intensity was not affected, but the intensity outside the Golgi was decreased. This is in line with our finding that loss of Vti1a/b differentially affected different compartments of the Golgi apparatus. Taken together, while the Golgi levels of proteins associated with DCVs were reduced in Vti1a/b deficient neurons, the impact on average staining intensities was different for each protein. This suggests that these proteins do not depend on Vti1a/b in the same way.

The effects of Vti1a/b DKO are not specific for DCVs, since LAMP1 staining patterns were also disturbed in Vti1a/b deficient neurons. This is not surprising, considering that many different Golgi proteins and the ER are impacted by loss of Vti1a/b. Even though there is no significant difference in Golgi export of constitutive cargo in Vti1a/b DKO neurons at a late timepoint, the export is initially slower[7]. Thus, loss of Vti1a/b affects more cellular trafficking routes than regulated secretion. This suggests that defective retrograde trafficking impacts multiple secretory pathways. In line with this suggestion, disturbing retrograde trafficking by knocking out any of the four subunits of the GARP complex also disrupts anterograde trafficking and affects Golgi morphology[24,36]. In addition, knockout or knockdown of any of the components of the COG complex similarly affects Golgi morphology and function and causes changes to the endolysosomal system[18,19]. Therefore, we conclude that disturbed retrograde trafficking affects Golgi morphology and function and thereby likely impacts many more Golgi-dependent processes than Golgi export of regulated cargo.

Disturbing membrane homeostasis by addition of ceramide or sphingosine produced similar Golgi abnormalities as observed in the absence of Vti1a/b. Disturbed membrane homeostasis can affect Golgi organization in different ways, for example by disrupting lipid rafts or by altering membrane permeability[37–39]. Since Vti1a/b are required for retrograde trafficking, Vti1a/b deficiency may directly affect recycling of membrane components to the Golgi apparatus, but Golgi abnormalities may also be an indirect effect of impaired recycling of membrane-processing enzymes. We focused on sphingomyelin synthases because it was shown that retrograde trafficking defects cause mislocalization of SMS1[20]. In addition, SMS1 and SMS2 are required for normal trafficking and secretion of insulin and vesicular stomatitis virus G protein tagged with GFP (VSVG-GFP)[40]. We did not observe abnormalities in localization of SMS1/2-GFP and SMS1/2 did not rescue Golgi abnormalities in Vti1a/b DKO neurons, nor did inhibition of de novo ceramide synthesis by myriocin application. This suggests that mislocalization of sphingomyelin synthases does not underly the defects in Vti1a/b deficient neurons. Since cells have many different ways to regulate ceramide levels[41], we cannot exclude that the Vti1a/b DKO Golgi phenotype is the result of defects in other aspects of lipid metabolism, but clear leads, as in the case of SMS1/2 and myriocin, are lacking, to our knowledge. Altogether, we have shown that Vti1a/b are important for different aspects of TGN and *cis*-/medial Golgi organization.

Methods

Laboratory animals and primary cultures. Animal experiments were approved by the animal ethical committee of the VU University/VU University Medical Centre (license number: FGA 11-03). Animals were bred and housed according to Institutional and Dutch governmental guidelines. All experiments were conducted in compliance with ARRIVE guidelines. Embryonic day (E) 18.5 Vti1a/b DKO, Vti1a/b DHZ and C57BL/6 mouse embryos were used for primary hippocampal or cortical culture. Vti1a/b DKO and DHZ mice have been described previously[7,42]. In total 70 litters of Vti1a/b mice were genotyped. DHZ were used as controls because of the low probability to obtain DKO and double-WT within one litter. If multiple pups in a litter were of the same genotype, their neurons were pooled. For experiments in wildtype neurons, 3 wildtype pups were used. Mouse hippocampi or cortices were dissected in Hanks' balanced salt solution (Sigma), supplemented with 10 mM HEPES (Gibco) and were digested with 0.25% trypsin (Gibco) in Hanks' + HEPES for 15 min at 37 °C. Hippocampi and cortices were washed three times with Hanks' + HEPES, once with DMEM complete (DMEM + Glutamax (Gibco), supplemented with 10% FCS (Gibco), 1% NEAA (Sigma) and 1% penicillin/streptomycin (Sigma)) and triturated with fire-polished Pasteur pipettes. Dissociated cells were spun down and resuspended in Neurobasal medium (Gibco) supplemented with 2% B-27 (Gibco), 1.8% HEPES, 0.25% Glutamax (Gibco) and 0.1% penicillin/streptomycin. Continental cultures were created by plating WT and Vti1a/b DHZ hippocampal neurons at 25 K/well and Vti1a/b DKO hippocampal neurons at 50 K/well. Neurons were seeded on pre-grown rat glia on 18 mm glass coverslips in 12 well plates. For Western Blot experiments, Vti1a/b DHZ and Vti1a/b DKO cortical neurons were plated at 300 k/well and 600 k/well, respectively, on 6 well plates coated with 0.0005% poly-l-ornithine (Sigma) and 2.5 µg/ml laminin (Sigma).

Immunocytochemistry. Neurons were fixed at DIV2 or DIV7/DIV8 in freshly prepared 3.7% paraformaldehyde (EMS) for 10 min at room temperature and permeabilized with 0.1% Triton X-100 (Fisher Scientific) for 10 min. In case only goat secondary antibodies were used, neurons were blocked with 5% normal goat serum (Life Technologies) for 30 min. Incubation with primary and secondary antibodies was done at room temperature for 1 h. All solutions were in PBS (composition in mM: 137 NaCl, 2.7 KCl, 10 Na_2HPO_4, 1.8 KH_2PO_4; pH = 7.4). Coverslips were mounted in Mowiol (Sigma). In case donkey anti-sheep and goat antibodies were combined, secondary antibody incubation was split into two steps to prevent cross-reaction: donkey anti-sheep antibodies were incubated for 1 h and after thorough washing and blocking with 5% normal goat serum, goat secondary antibodies were incubated for 1 h.

Primary antibodies used for immunocytochemistry: GM130 (1:500, BD, 610822), giantin (1:200, BioLegend, 909701), TGN38 (1:100, BioRad, AHP499G), TMEM87A (1:100, Novus Biologicals, NBP1-90532), ARL1 (1:50, Santa Cruz, sc-393785), HID1 (1:100, Novus Biologicals, NBP2-02667), CCDC186 (1:200, Novus Biologicals, NBP1-90440), CgB (1:500, Synaptic Systems, 259 103), LAMP1 (1:500, Abcam, ab25245), Golgin97 (1:50, Santa Cruz, sc-59820), KDEL (1:100, Enzo, ADI-SPA-827), gamma-adaptin (1:250, BD, 610385). Secondary antibodies were AlexaFluor-conjugated (1:500, Invitrogen) or STAR GREEN-, STAR580- or STAR635p-conjugated (1:100, Abberior).

For ceramide and sphingosine experiments, DIV7 neurons were treated with 20 µM C6-Ceramide (Cayman Chemical), 8 µM L-Erythro-Sphingosine (Cayman Chemical) or 0.1% DMSO (Sigma) for 4 h. For myriocin experiments, 50 µM myriocin (Cayman Chemical) or 0.1% DMSO was added to neurons 4 h after plating and neurons were fixed at DIV8.

Confocal imaging was performed on a Leica TCS SP8 STED 3× microscope (Leica Microsystems) with LAS X acquisition software, using a 100× oil objective (NA = 1.4). A pulsed white light laser was used to excite the samples. The signal was detected using a gated hybrid detector (HyD) (Leica Microsystems) in photon-counting mode.

Images were analyzed in Fiji software[43]. The BAR plugin was used to plot multichannel profiles in order to analyze the distance between peaks of Golgi proteins[44].

Western blot. Neurons were lysed in Laemmli buffer (2% SDS, 10% glycerol, 500 mM DTT, 62.5 mM Tris–HCl, and 0.01% Bromophenol Blue; pH 6.8) at DIV7. Samples were separated on SDS–polyacrylamide gels or 4–20% gradient gel (Biorad, #4568094) and transferred to nitrocellulose or PVDF membranes. Blots were blocked in 2.5% bovine serum albumin (BSA) for 1 h at 4 °C and incubated with primary antibodies at 4 °C overnight (gamma-adaptin (1:500), Golgin97 (1:200) and CCDC186 (1:1000)). Secondary antibodies were incubated for 1 h at RT. Blots were scanned using a Fuji Film FLA 5000. Blocking and antibody solutions were prepared in PBS containing 0.1% Tween-20. Total protein levels were measured using 2,2,2-Trichloroethanol.

Plasmids. NPY-SEP plasmid has been described before[45]. TGN38-GFP, SMS1-GFP and SMS2-GFP were generated by amplifying TGN38, SMS1 and SMS2 from a mouse cDNA library and tagging them with eGFP at the C-terminus. The following primers were used for amplification of TGN38: gctcaccatgatcccaagctttaggttcaaacgttgg and cggtaccgcgggcccatgcggttccaggttgcg; SMS1: ggactcagatctcgaatgttgtctgccaggaccatgaaggaag and gaagcttgagctcgattatgtgtcgtttaccagccggctatatttaacttgcctactaaggt; SMS2: ggactcagatctcgaatggatatcatagagacagcaaaacttgaaggtcacttgg and gaagcttgagctcgatcaggtagacttctcattatcctccccgatcttctgg) These plasmids were cloned into lentiviral vectors under human Synapsin promoter and viral particles were delivered to neurons at DIV3 or DIV4 for NPY-SEP and TGN38-GFP and DIV0 for SMS1-GFP and SMS2-GFP.

Statistical analysis. Statistical analysis and graphing were performed using GraphPad Prism 7. Shapiro–Wilk was used to test distribution normality. When assumption of normality was met, parametric tests were used: two-tailed *t*-test or ANOVA (with Tukey's multiple comparisons test). Otherwise, non-parametric tests

were used: two-tailed Mann Whitney or Kruskall-Wallis (with Dunn's multiple comparisons test). Significance was accepted at $p < 0.05$. Each data point represents one cell and bars show mean ± SEM. All data and statistical tests used are summarized in Supplementary Table 1. No sample size calculation was performed. No randomization or blinding was performed. Neurons were excluded from analysis if neuronal Golgi area could not be determined, for example because it was overlapping with glial Golgi.

Data availability

The data generated and analyzed during the current study are included in this published article and its supplementary information files. Datasets are available from the corresponding author on request.

Received: 15 July 2022; Accepted: 28 November 2022
Published online: 02 December 2022

References

1. Bramham, C. R. & Messaoudi, E. BDNF function in adult synaptic plasticity: The synaptic consolidation hypothesis. *Prog. Neurobiol.* **76**, 99–125 (2005).
2. Comeras, L. B., Herzog, H. & Tasan, R. O. In *Ann N Y Acad Sci, vol. 1455* 59–80 (Blackwell Publishing Inc., 2019).
3. Zi, Z. L. *et al.* A trans-Golgi network golgin is required for the regulated secretion of TNF in activated macrophages in vivo. *Proc. Natl. Acad. Sci. USA* **105**, 3351–3356 (2008).
4. Alldredge, B. Pathogenic involvement of neuropeptides in anxiety and depression. *Neuropeptides* **44**, 215–224 (2010).
5. Sah, R. & Geracioti, T. D. Neuropeptide y and posttraumatic stress disorder. *Mol. Psychiatry* **18**, 646–655 (2013).
6. Kim, T., Gondré-Lewis, M. C., Arnaoutova, I. & Loh, Y. P. Dense-core secretory granule biogenesis. *Physiology* **21**, 124–133 (2006).
7. Emperador-Melero, J. *et al.* Vti1a/b regulate synaptic vesicle and dense core vesicle secretion via protein sorting at the Golgi. *Nat. Commun.* **9**, 1 (2018).
8. Ma, C. I. J. *et al.* An early endosome-derived retrograde trafficking pathway promotes secretory granule maturation. *J. Cell Biol.* **219**, 3 (2020).
9. Reaves, B., Horn, M. & Banting, G. TGN38/41 recycles between the cell surface and the TGN: Brefeldin A affects its rate of return to the TGN. *Mol. Biol. Cell* **4**, 93–105 (1993).
10. McNamara, J. O., Grigston, J. C., VanDongen, H. M. A. & VanDongen, A. M. J. Rapid dendritic transport of TGN38, a putative cargo receptor. *Mol. Brain Res.* **127**, 68–78 (2004).
11. De Wit, J., Toonen, R. F. & Verhage, M. Matrix-dependent local retention of secretory vesicle cargo in cortical neurons. *J. Neurosci.* **29**, 23–37 (2009).
12. Arora, S. *et al.* SNAP-25 gene family members differentially support secretory vesicle fusion. *J. Cell Sci.* **130**, 1877–1889 (2017).
13. Hummer, B. H. *et al.* HID-1 controls formation of large dense core vesicles by influencing cargo sorting and trans-Golgi network acidification. *Mol. Biol. Cell* **28**, 3870–3880 (2017).
14. Cattin-Ortolá, J. *et al.* CCDC186 controls dense-core vesicle cargo sorting by exit. *bioRxiv* **2019**, 616458. https://doi.org/10.1101/616458 (2019).
15. Santos, T. C., Wierda, K., Broeke, J. H., Toonen, R. F. & Verhage, M. Early Golgi abnormalities and neurodegeneration upon loss of presynaptic proteins Munc18-1, Syntaxin-1, or SNAP-25. *J. Neurosci.* **37**, 4525–4539 (2017).
16. Hu, W. *et al.* Golgi fragmentation is associated with ceramide-induced cellular effects. *Mol. Biol. Cell* **16**, 1555–1567 (2005).
17. Fukunaga, T. *et al.* Implication of sphingolipid metabolism in the stability of the Golgi apparatus. *J. Cell Sci.* **113**, 3299–3307 (2000).
18. Blackburn, J. B., D'Souza, Z. & Lupashin, V. V. Maintaining order: COG complex controls Golgi trafficking, processing, and sorting. *FEBS Lett.* **593**, 2466–2487 (2019).
19. Shestakova, A., Zolov, S. & Lupashin, V. COG complex-mediated recycling of golgi glycosyltransferases is essential for normal protein glycosylation. *Traffic* **7**, 191–204 (2006).
20. Spessott, W., Uliana, A. & MacCioni, H. J. F. Cog2 null mutant CHO cells show defective sphingomyelin synthesis. *J. Biol. Chem.* **285**, 41472–41482 (2010).
21. Yeang, C., Ding, T., Chirico, W. J. & Jiang, X. C. Subcellular targeting domains of sphingomyelin synthase 1 and 2. *Nutr. Metab. (Lond.)* **8**, 1–9 (2011).
22. Huitema, K., Van Den Dikkenberg, J., Brouwers, J. F. H. M. & Holthuis, J. C. M. Identification of a family of animal sphingomyelin synthases. *EMBO J.* **23**, 33–44 (2004).
23. Pérez-Victoria, F. J., Mardones, G. A. & Bonifacino, J. S. Requirement of the human GARP complex for mannose 6-phosphate-receptor- dependent sorting of cathepsin D to lysosomes. *Mol. Biol. Cell* **19**, 2350–2362 (2008).
24. Schmitt-John, T. VPS54 and the wobbler mouse. *Front. Neurosci.* **9**, 381 (2015).
25. Fröhlich, F. *et al.* The GARP complex is required for cellular sphingolipid homeostasis. *Elife* **4**, 2514 (2015).
26. Petit, C. S. *et al.* Inhibition of sphingolipid synthesis improves outcomes and survival in GARP mutant wobbler mice, a model of motor neuron degeneration. *Proc. Natl. Acad. Sci. USA* **117**, 10565–10574 (2020).
27. Goud, B. & Gleeson, P. A. TGN golgins, rabs and cytoskeleton: Regulating the golgi trafficking highways. *Trends Cell Biol.* **20**, 329–336 (2010).
28. Lippincott-Schwartz, J. *et al.* Brefeldin A's effects on endosomes, lysosomes, and the TGN suggest a general mechanism for regulating organelle structure and membrane traffic. *Cell* **67**, 601–616 (1991).
29. Zulkefli, K. L. *et al.* A role for Rab30 in retrograde trafficking and maintenance of endosome-TGN organization. *Exp. Cell Res.* **399**, 112442 (2021).
30. Lu, L., Horstmann, H., Ng, C. & Hong, W. Regulation of Golgi structure and function by ARF-like protein 1 (Arl1). *J. Cell Sci.* **114**, 4543–4555 (2001).
31. Subramaniam, V. N., Peter, F., Philp, R., Wong, S. H. & Hong, W. GS28, a 28-kilodalton Golgi SNARE that participates in ER-Golgi transport. *Science* **272**, 1161–1163 (1996).
32. Subramaniam, V. N. *et al.* Monoclonal antibody HFD9 identifies a novel 28 kDa integral membrane protein on the cis-Golgi. *J. Cell Sci.* **108**, 2405–2414 (1995).
33. Chia, J. *et al.* RNAi screening reveals a large signaling network controlling the Golgi apparatus in human cells. *Mol. Syst. Biol.* **8**, 629 (2012).
34. Yoo, S. H. *et al.* Localization of the secretory granule marker protein chromogranin B in the Nucleus: Potential role in transcription control *. *J. Biol. Chem.* **277**, 16011–16021 (2002).
35. Du, W. *et al.* HID-1 is required for homotypic fusion of immature secretory granules during maturation. *Elife* **5**, 2165 (2016).
36. Hirata, T. *et al.* Post-Golgi anterograde transport requires GARP-dependent endosome-to-TGN retrograde transport. *Mol. Biol. Cell* **26**, 3071–3084 (2015).
37. Pascher, I. Molecular arrangements in sphingolipids conformation and hydrogen bonding of ceramide and their implication on membrane stability and permeability. *Biochim. Biophys. Acta (BBA) Biomembr.* **455**, 433–451 (1976).

38. Bieberich, E. Sphingolipids and lipid rafts: Novel concepts and methods of analysis. *Chem. Phys. Lipids* **216**, 114–131 (2018).
39. Tracey, T. J., Steyn, F. J., Wolvetang, E. J. & Ngo, S. T. Neuronal lipid metabolism: Multiple pathways driving functional outcomes in health and disease. *Front. Mol. Neurosci.* **11**, 2569 (2018).
40. Subathra, M., Qureshi, A. & Luberto, C. Sphingomyelin synthases regulate protein trafficking and secretion. *PLoS ONE* **6**, e23644 (2011).
41. Hussain, M. M., Jin, W. & Jiang, X. C. Mechanisms involved in cellular ceramide homeostasis. *Nutr. Metab. (Lond.)* **9**, 1–7 (2012).
42. Kunwar, A. J. *et al.* Lack of the endosomal SNAREs vti1a and vti1b led to significant impairments in neuronal development. *Proc. Natl. Acad. Sci. USA* **108**, 2575–2580 (2011).
43. Schindelin, J. *et al.* Fiji: An open-source platform for biological-image analysis. *Nat. Methods* **9**, 676–682 (2012).
44. Ferreira, T., Miura, K., Chef, B. & Eglinger, J. In *Scripts: BAR 1.1.6.* (2015). 10.5281/ZENODO.28838.
45. van de Bospoort, R. *et al.* Munc13 controls the location and efficiency of dense-core vesicle release in neurons. *J. Cell Biol.* **199**, 883–891 (2012).

Acknowledgements

We thank Ingrid Saarloos and Robbert Zalm for cloning and producing viral particles; Lisa Laan, Ingrid Saarloos and Desiree Schut for producing glia and for primary culture assistance; Ingrid Saarloos for Western blotting; Joke Wortel for animal breeding; Joost Hoetjes for genotyping; and members of the Center for Neurogenomics and Cognitive Research DCV project team for fruitful discussions. We acknowledge the Microscopy and Cytometry Core Facility at the Amsterdam UMC—Location VUmc for providing assistance in microscopy. This work is supported by a European Research Council Advanced Grant (322966) of the European Union (to M.V.).

Author contributions

D.V.B. performed experiments and analyzed the data. D.V.B., R.F.T. and M.V. designed the research and wrote the paper.

Competing interests

The authors declare no competing interests.

Additional information

Supplementary Information The online version contains supplementary material available at https://doi.org/10.1038/s41598-022-25331-x.

Correspondence and requests for materials should be addressed to M.V.

Reprints and permissions information is available at www.nature.com/reprints.

Publisher's note Springer Nature remains neutral with regard to jurisdictional claims in published maps and institutional affiliations.